Three-dimensional non-Abelian generalizations of the Hofstadter model: Spin-orbit-coupled butterfly trios

Vincent Liu,[1,2,*] Yi Yang,[1,3,†] John D. Joannopoulos,[1] and Marin Soljačić[1]

[1]*Research Laboratory of Electronics and Department of Physics, Massachusetts Institute of Technology, Cambridge, Massachusetts 02139, USA*

[2]*Department of Physics, University of California, Berkeley, California 94720, USA*

[3]*Department of Physics, The University of Hong Kong, Hong Kong, China*

(Received 21 June 2021; accepted 18 August 2021; published 15 September 2021)

We theoretically introduce and study a three-dimensional Hofstadter model with linearly varying non-Abelian gauge potentials along all three dimensions. The model can be interpreted as spin-orbit coupling among a trio of Hofstadter butterfly pairs since each Cartesian surface (*xy*, *yz*, or *zx*) of the model reduces to a two-dimensional non-Abelian Hofstadter problem. By evaluating the commutativity among arbitrary loop operators around all axes, we derive its genuine (necessary and sufficient) non-Abelian condition, namely, that at least two out of the three hopping phases should be neither 0 nor π. Under different choices of gauge fields in either the Abelian or the non-Abelian regime, both weak and strong topological insulating phases are identified in the model.

DOI: 10.1103/PhysRevB.104.115127

I. INTRODUCTION

The Hofstadter model [1] is fundamental to the study of the quantum Hall effect and topology in condensed matter physics. It describes noninteracting electrons hopping in a two-dimensional square lattice under a perpendicular U(1) magnetic field. In solid state systems, the magnetic fields required for realizing the Hofstadter model had been inaccessible experimentally until the introduction of moiré superlattices [2–4], which expand the size of unit cells and the threaded magnetic flux substantially.

An alternative way to realize the Hofstadter model in real space is via synthetic gauge fields [5] in artificial, engineered systems. So far, a plethora of realizations have been achieved, including microwave scatterers [6], cold atoms [7,8], acoustics [9], photons [10], and superconducting qubits [11,12].

In two dimensions, there has been considerable interest in studying non-Abelian generalizations of the Hofstadter model, which replace the Abelian U(1) gauge fields with non-Abelian choices. Categorized by the spatial arrangements of the gauge fields, there have been theoretical studies that feature constant [13–16] and linearly varying non-Abelian gauge fields in one [17] or two [18] spatial dimensions. Experimentally, real-space building blocks of non-Abelian SU(2) gauge fields were demonstrated [19] in photonics via minimal-scheme, non-Abelian Aharonov-Bohm interference [20–22]. In addition, non-Abelian braiding of topological zero modes was proposed and realized with coupled waveguide arrays [23,24]. These advances indicate a possibility to realize non-Abelian Hofstadter models in photonic systems.

In three dimensions (3D), Abelian generalizations of the Hofstadter model corresponding to tilted magnetic fields have been studied as many as three decades ago [25–28]. In particular, such a 3D problem with arbitrarily oriented three-dimensional flux states can be reduced to a one-dimensional hopping in a suitably chosen gauge [27]. Moreover, the model was found to support the 3D quantum Hall effect with quantized Hall conductance under anisotropic conditions [29]. Far fewer non-Abelian generalizations have been considered in 3D. Specifically, a 3D Hofstadter-like problem with non-Abelian gauge potentials that vary linearly along a single direction [of the remaining two directions, one has a constant SU(2) gauge and the other a real hopping] has been studied [30], which is shown to also be reducible to an effective 1D problem.

In this paper, we theoretically propose and study a 3D non-Abelian Hofstadter model on a cubic lattice, whose non-Abelian SU(2) gauge potentials are linearly varying along all three dimensions. A crucial feature of our model construction is that any arbitrary Cartesian surface (either *xy*, *yz*, or *zx*) of our 3D model reduces to a two-dimensional non-Abelian Hofstadter model in the symmetric gauge [18]. Meanwhile, adjacent layers are coupled with spatially varying hopping. Therefore, the whole system can be treated as the spin-orbit coupling among three Hofstadter butterflies (each encoded along a single dimension). By evaluating the commutativity between arbitrary real-space loop operators, we derive the necessary and sufficient condition for our model to be genuinely non-Abelian, namely, that at least two out of the three hopping phases are neither 0 nor π. Compared to the 3D Abelian Hofstadter model, the spin-orbit coupling in the 3D non-Abelian Hofstadter model opens new band gaps. We further show that these gaps can be of either weak or strong 3D $\mathbb{Z}_2$ topological insulating phases under different choices of the gauge potentials.

*vincent_liu@berkeley.edu
†yiy@mit.edu

II. MODELS

As a warmup, we begin by describing homogeneous magnetic fields in 3D cubic lattices labeled by (m, n, l). First, homogeneous U(1) magnetic fields in three dimensions can be described by three-dimensional Hofstadter models. In a general form that is akin to our proposed model below, the 3D Abelian Hofstadter model [25–29] can be expressed as

$$\begin{aligned} H_1 = &- \sum_{m,n,l} t_x c^\dagger_{m+1,n,l} e^{i(l\pm n)\theta_x} c_{m,n,l} \\ &+ t_y c^\dagger_{m,n+1,l} e^{i(m\pm l)\theta_y} c_{m,n,l} \\ &+ t_z c^\dagger_{m,n,l+1} e^{i(n\pm m)\theta_z} c_{m,n,l} + \text{H.c.}, \end{aligned} \tag{1}$$

where θ_x, θ_y, and θ_z are hopping phases and t_x, t_y, and t_z are hopping amplitudes along three directions. H_1 corresponds to a gauge potential $\mathbf{A}_1 = [(l \pm n)\theta_x, (m \pm l)\theta_y, (n \pm m)\theta_z]$, which varies linearly along all three dimensions. The associated magnetic flux can be evaluated from the loop operator along different Cartesian surfaces, which yields a magnetic field of $\mathbf{B}_1 = (\theta_y \mp \theta_x, \theta_x \mp \theta_z, \theta_z \mp \theta_y)$. Evidently, the choice of $\pm$ in Eq. (1) corresponds to different homogeneous magnetic fields [see Supplemental Material [31] Figs. S1(b) and S1(d)].

On the other hand, a homogeneous non-Abelian SU(2) gauge potential and its associated Hamiltonian on a cubic lattice are given by

$$\begin{aligned} H_2 = &- \sum_{m,n,l} t_x c^\dagger_{m+1,n,l} e^{i\theta_x\sigma_x} c_{m,n,l} \\ &+ t_y c^\dagger_{m,n+1,l} e^{i\theta_y\sigma_y} c_{m,n,l} \\ &+ t_z c^\dagger_{m,n,l+1} e^{i\theta_z\sigma_z} c_{m,n,l} + \text{H.c.}, \end{aligned} \tag{2}$$

which corresponds to a gauge potential $\mathbf{A}_2 = (\theta_x\sigma_x, \theta_y\sigma_y, \theta_z\sigma_z)$, where $\sigma_{x,y,z}$ are Pauli matrices. Every layer of H_2 becomes the celebrated 2D homogeneous non-Abelian model as proposed in Refs. [17,32]. The 3D non-Abelian gauge potential $\mathbf{A}_2$ describes a spatially homogeneous SU(2) magnetic field $\mathbf{B}_2 = (2\theta_y\theta_z\sigma_x, 2\theta_z\theta_x\sigma_y, 2\theta_x\theta_y\sigma_z)$. The associated Bloch Hamiltonian of H_2 is given by

$$h_2(\mathbf{k}) = 2\sum_i \cos k_i \cos\theta_i\sigma_0 - 2\sum_i \sin k_i \sin\theta_i\sigma_i. \tag{3}$$

This two-band Hamiltonian is time-reversal symmetric and always gapless. It hosts Weyl points at the eight time-reversal-invariant momenta (TRIMs).

We propose a 3D non-Abelian Hofstadter model inspired by Eqs. (1) and (2). Specifically, we insert the three Pauli matrices from Eq. (2) into the complex hopping phases in Eq. (1) along the three directions. This replacement leads to inhomogeneous, Hofstadter-Harper-like non-Abelian gauge potentials in 3D,

$$\mathbf{A}_\pm = [(l \pm n)\theta_x\sigma_x, (m \pm l)\theta_y\sigma_y, (n \pm m)\theta_z\sigma_z]. \tag{4}$$

The associated Hamiltonian (see Fig. 1) is given by

$$\begin{aligned} H_\pm(\theta_x, \theta_y, \theta_z) = &- \sum_{m,n,l} t_x c^\dagger_{m+1,n,l} e^{i(l\pm n)\theta_x\sigma_x} c_{m,n,l} \\ &+ t_y c^\dagger_{m,n+1,l} e^{i(m\pm l)\theta_y\sigma_y} c_{m,n,l} \\ &+ t_z c^\dagger_{m,n,l+1} e^{i(n\pm m)\theta_z\sigma_z} c_{m,n,l} + \text{H.c.}. \end{aligned} \tag{5}$$

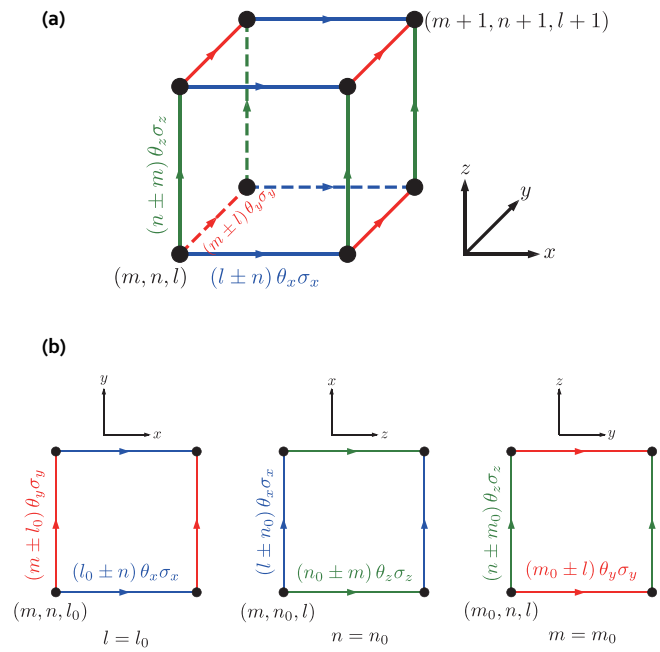

FIG. 1. Three-dimensional non-Abelian generalization of the Hofstadter model: the blue, red, and green colors represent the link variables in the x, y, and z directions. (a) Schematic of our three-dimensional model. (b) Cartesian surface cuts of our model. Each Cartesian cut corresponds to a two-dimensional Hofstadter non-Abelian model in the symmetric gauge.

Throughout this work, we assume that $t_x = t_y = t_z = 1$. Similar to Eq. (1), the choice of $\pm$ corresponds to different magnetic fields and thus different eigenstates [see Supplemental Material [31] Figs. S1(a) and S1(c)]. A crucial feature of $H_\pm$ is that every one of its 2D Cartesian surfaces (along the xy, zx, and yz planes) reduces to a 2D non-Abelian Hofstadter model [18] [see Fig. 1(b)]. Meanwhile, all layers, along all three directions, are stacked and connected with complex non-Abelian hoppings. As a result, the system contains spin-orbit coupling among a trio of Hofstadter butterfly pairs.

Analogous to the original Hofstadter model, this three-dimensional non-Abelian system can be solved in an enlarged magnetic unit cell if θ_x, θ_y, and θ_z are rational multiples of 2π, i.e., $\theta_x = 2\pi\, p_x/q_x$, $\theta_y = 2\pi\, p_y/q_y$, and $\theta_z = 2\pi\, p_z/q_z$ (where p_i and q_i are coprime). The size of the magnetic unit cell is $\text{lcm}(q_y, q_z) \times \text{lcm}(q_x, q_z) \times \text{lcm}(q_x, q_y) \equiv Q_x \times Q_y \times Q_z$, where lcm denotes the least common multiple. Consequently, the associated magnetic Brillouin zone is $k_x \in [0, 2\pi/Q_x)$, $k_y \in [0, 2\pi/Q_y)$, $k_z \in [0, 2\pi/Q_z)$.

III. GENUINE NON-ABELIAN CONDITIONS

Although $H_\pm$ is non-Abelian in general, there are situations (e.g., the obvious case $\theta_x = \theta_y = \theta_z = 0$) when the model reduces to Abelian. Therefore, to obtain the necessary and sufficient condition under which the models are genuinely non-Abelian [18,33], we examine the commutativity of unit plaquette loop operators at arbitrary lattice sites in three directions,

$$W^{\mu\nu}_{\mathbf{r}} = U^\dagger_\nu(\mathbf{r}) U^\dagger_\mu(\mathbf{r} + \hat{e}_\nu) U_\nu(\mathbf{r} + \hat{e}_\mu) U_\mu(\mathbf{r}), \tag{6}$$

where $\{\mu, \nu\} = \{x, y, z\}$, $\hat{e}_\mu$ is the unit vector in the μ direction, and we adopt the counterclockwise convention.

Specifically, the loop operators for a unit plaquette at site $\mathbf{r} = (m, n, l)$ are given by

$$\boldsymbol{W}^{xy,\pm}_{\mathbf{r}} = \Theta_y^{-(m\pm l)}\Theta_x^{-[l\pm(n+1)]}\Theta_y^{m+1\pm l}\Theta_x^{l\pm n}, \tag{7a}$$

$$\boldsymbol{W}^{zx,\pm}_{\mathbf{r}} = \Theta_x^{-(l\pm n)}\Theta_z^{-[n\pm(m+1)]}\Theta_x^{l+1\pm n}\Theta_z^{n\pm m}, \tag{7b}$$

$$\boldsymbol{W}^{yz,\pm}_{\mathbf{r}} = \Theta_z^{-(n\pm m)}\Theta_y^{-[m\pm(l+1)]}\Theta_z^{n+1\pm m}\Theta_y^{m\pm l}, \tag{7c}$$

where $\Theta_x^m \equiv \exp(im\theta_x\sigma_x)$, $\Theta_y^m \equiv \exp(im\theta_y\sigma_y)$, and $\Theta_z^m \equiv \exp(im\theta_z\sigma_z)$. We also define $\Theta_x \equiv \Theta_x^1$, $\Theta_y \equiv \Theta_y^1$, and $\Theta_z \equiv \Theta_z^1$ for compact notation. $\pm$ in the superscript denotes the choice of gauge fields in Eq. (4). We prove below that both H_+ and H_- reduce to Abelian, i.e., Eqs. (7) are Abelian, if and only if

$$\text{at least two of } \theta_x, \theta_y, \text{ and } \theta_z \text{ are either 0 or } \pi. \tag{8}$$

We consider loop operators near $\mathbf{R} = \mathbf{0}$ for H_-, which are given by

$$W^{xy,-}_{0,0,0} = \Theta_x^{\mp1}\Theta_y, \quad W^{xy,-}_{0,0,\mp1} = \Theta_y\Theta_x^{\mp1}, \quad W^{zx,-}_{0,0,0} = \Theta_z^{\mp1}\Theta_x,$$
$$W^{zx,-}_{0,\mp1,0} = \Theta_x\Theta_z^{\mp1}, \quad W^{yz,-}_{0,0,0} = \Theta_y^{\mp1}\Theta_z, \quad W^{yz,-}_{\mp1,0,0} = \Theta_z\Theta_y^{\mp1}. \tag{9}$$

To derive a necessary condition, we note that all of these loop operators must commute. Since these loop operators deal with permutations of θ_x, θ_y, and θ_z, we adopt $\{a, b, c\} \in \{x, y, z\}$ to denote their permutations. Equation (9) requires

$$[\Theta_a\Theta_b, \Theta_c\Theta_a] = 0. \tag{10}$$

We can evaluate this commutator explicitly as

$$\begin{aligned}&-2\epsilon_{abc}\cos(2\theta_a)\sin(\theta_b)\sin(\theta_c)\sigma_a + [2\sin^2(\theta_a)\sin(\theta_b)\cos(\theta_c) + 2\epsilon_{abc}\sin(\theta_a)\cos(\theta_a)\cos(\theta_b)\sin(\theta_c)]\sigma_b\\ &+ [2\sin^2(\theta_a)\cos(\theta_b)\sin(\theta_c) + 2\epsilon_{abc}\sin(\theta_a)\cos(\theta_a)\sin(\theta_b)\cos(\theta_c)]\sigma_c = 0,\end{aligned} \tag{11}$$

where ϵ_{abc} is the Levi-Civita symbol. The coefficients for all Pauli matrices must vanish to satisfy Eq. (10). Taken together, we must have

$$\cos(2\theta_a)\sin(\theta_b)\sin(\theta_c) = 0, \tag{12a}$$

$$\sin^2(\theta_a)\sin(\theta_b)\cos(\theta_c) = 0, \tag{12b}$$

$$\sin^2(\theta_a)\cos(\theta_b)\sin(\theta_c) = 0. \tag{12c}$$

Two situations arise: $\sin(\theta_a) = 0$ or $\sin(\theta_a) \neq 0$.

If $\sin(\theta_a) = 0$, $\cos(2\theta_a) \neq 0$, at least one of $\sin(\theta_b)$ and $\sin(\theta_c)$ is 0 by Eq. (12a). Thus, at least two of θ_a, θ_b, and θ_c are either 0 or π. This is a necessary condition.

If $\sin(\theta_a) \neq 0$, Eqs. (12b) and (12c) imply that either $\sin(\theta_b) = \sin(\theta_c) = 0$ or $\cos(\theta_b) = \cos(\theta_c) = 0$. The former condition is equivalent to the necessary condition above. For the latter, $\sin(\theta_b)\sin(\theta_c) \neq 0$ requires $\cos(2\theta_a) = 0$ [as per Eq. (12a)], i.e., $\cos(2\theta_x) = \cos(2\theta_y) = \cos(2\theta_z) = 0$. As a result, we can no longer satisfy $\cos(\theta_b) = \cos(\theta_c) = 0$. Thus, the latter case results in a contradiction.

So far, we have proven that our condition Eq. (8) is necessary for H_- to be Abelian. We now examine H_+. In this case, the operators are in the form $\Theta_a^{-1}\Theta_b$ or $\Theta_b\Theta_a^{-1}$. The associated loop operators must commute, i.e., $[\Theta_a^{-1}\Theta_b, \Theta_c^{-1}\Theta_a] = 0$ for all choices of distinct a, b, and c. We again evaluate the commutator explicitly:

$$\begin{aligned}&2\epsilon_{abc}\sin(\theta_b)\sin(\theta_c)\sigma_a + [-2\sin^2(\theta_a)\sin(\theta_b)\cos(\theta_c) + 2\epsilon_{abc}\sin(\theta_a)\cos(\theta_a)\cos(\theta_b)\sin(\theta_c)]\sigma_b\\ &+ [2\sin^2(\theta_a)\cos(\theta_b)\sin(\theta_c) + 2\epsilon_{abc}\sin(\theta_a)\cos(\theta_a)\sin(\theta_b)\cos(\theta_c)]\sigma_c = 0.\end{aligned} \tag{13}$$

We can follow the same arguments as those for H_- to arrive at the same necessary condition.

Therefore, we have proven that at least two of θ_x, θ_y, and θ_z being either 0 or π is a necessary Abelian condition. To prove it is also a sufficient condition, let θ_a and θ_b be 0 or π. Θ_a^n and Θ_b^n consequently reduce to ±1 for any integer n, which always commute with arbitrary SU(2) phase factors. The remaining link variables Θ_c^n are an Abelian group as they are exponentials of a single Pauli matrix. Taken together, the necessary condition is also sufficient, rendering it the genuine Abelian condition of $H_\pm$. Recalling that the genuine non-Abelian condition of the associated 2D model [18] requires nondivisibility of the gauge potentials by π, the 3D model studied here therefore becomes genuinely Abelian if at least one of its Cartesian surfaces [see Fig. 1(b)] is Abelian.

IV. GAPPED PHASES

$H_\pm$ obeys time-reversal symmetry $i\sigma_y K$ and inversion symmetry P. Therefore, its spectrum consists of Kramers doublets in the entire magnetic Brillouin zone (MBZ). As the cubic lattices are bipartite, the model obeys a sublattice symmetry that maps $E(k_x, k_y, k_z) \to -E(k_x + \pi, k_y + \pi, k_z + \pi)$. When at least one of q_x, q_y, and q_z is even, i.e., $q_xq_yq_z$ is even, $H_\pm$ also respects chiral symmetry, which we prove by leveraging the Harper equation of $H_\pm$ in Supplemental Material [31] Sec. S2. We obtain the explicit form of the chiral operator as follows. Without loss of generality, we assume $Q_x = \mathrm{lcm}(q_y, q_z)$ is even. The chiral operator S_x is

$$(S_xu)_{m,n,l} = (-1)^{m+n\alpha_{xy}+l\alpha_{xz}}(i)^{Q_x/2}\sigma_0u_{m+Q_x/2,n,l}, \tag{14}$$

TABLE I. The strong and weak $\mathbb{Z}_2$ indices for $(\theta_x, \theta_y, \theta_z) = (0, \pi, 2\pi/3)$ for the lowest two gaps are shown. The $\mathbb{Z}_2$ indices for the two higher gaps follow by chiral symmetry.

Gap	Bands	ν_0	ν_1	ν_2	ν_3
1	12	0	0	0	0
2	24	0	0	1	0

where u is the wave function. Here, we define $\alpha_{\mu\nu} \equiv (Q_\mu p_\nu / q_\nu + 1) \mod 2$. S_y and S_z can be defined similarly if Q_y and Q_z are respectively even. The form of this 3D chiral operator is reminiscent of those in the 2D Abelian [34] and non-Abelian [18] Hofstadter models.

Finding the eigenspectrum of the model is computationally expensive as the system size increases rapidly with q_x, q_y, and q_z—the size of the magnetic unit cell is $\mathrm{lcm}(q_y, q_z) \times \mathrm{lcm}(q_z, q_x) \times \mathrm{lcm}(q_x, q_y)$. In the following, we focus on H_+. We study two choices of gauge fields, $(\theta_x, \theta_y, \theta_z) = (0, \pi, 2\pi/3)$ and $(\theta_x, \theta_y, \theta_z) = (2\pi/3, 2\pi/3, 0)$, which lie within the Abelian and non-Abelian regimes respectively, according to our genuine condition proven above. For $H_+(0, \pi, 2\pi/3)$, the magnetic unit cell has a dimension of $6 \times 3 \times 2$ for a total of 72 bands, i.e., 36 Kramers partners. This choice of gauge fields lies within the Abelian regime:

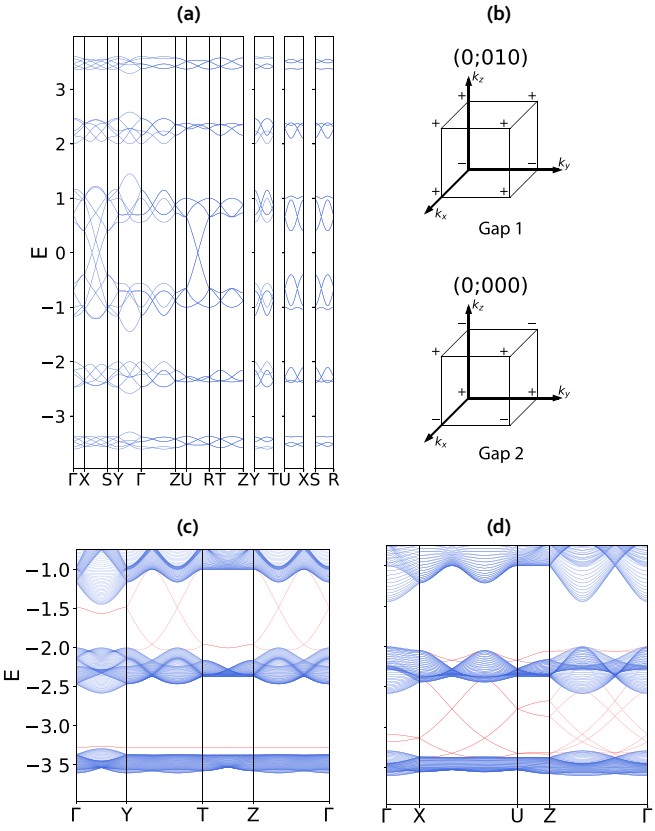

FIG. 2. (a) Bulk band structure of our model with $(\theta_x, \theta_y, \theta_z) = (0, \pi, 2\pi/3)$ sampled along paths between high-symmetry points in the MBZ. (b) Inversion eigenvalues at TRIMs. (c), (d) Surface band structure of the model cut along the (c) x and (d) y directions (with 20 magnetic unit cells). Surface states are highlighted in red.

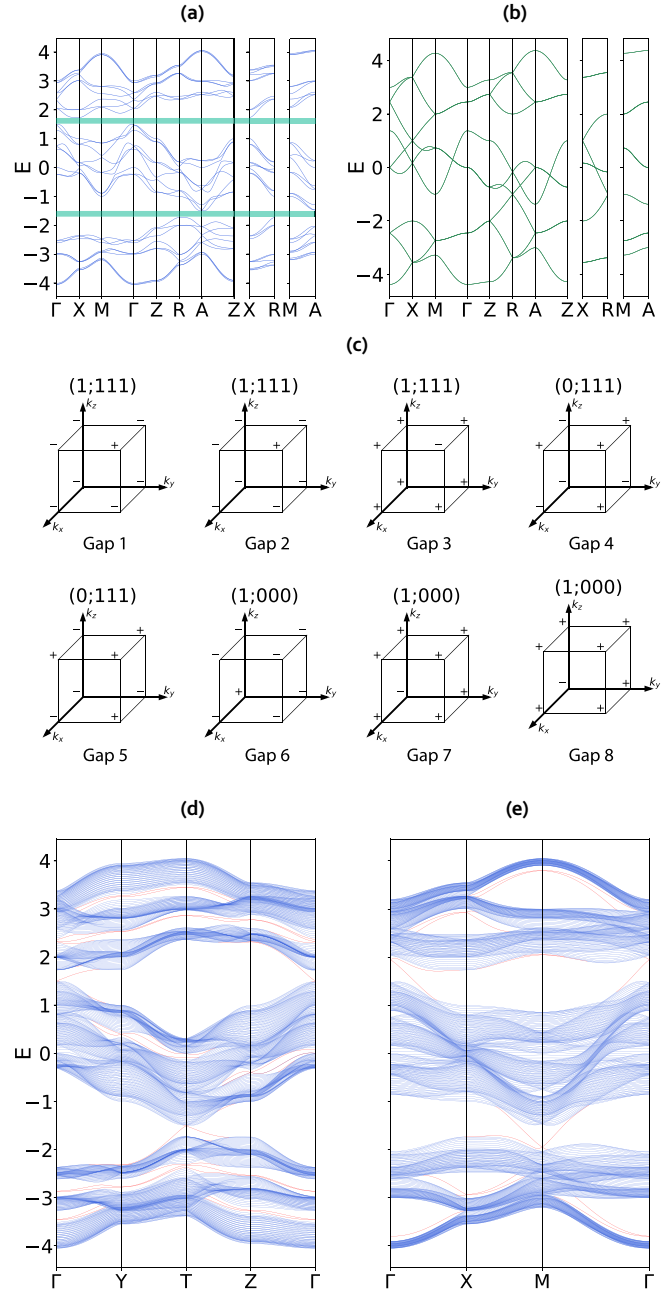

FIG. 3. (a), (b) Bulk band structure of the (a) non-Abelian and (b) Abelian models with the choice of gauge fields $(\theta_x, \theta_y, \theta_z) = (2\pi/3, 2\pi/3, 0)$, sampled along paths between high-symmetry points in the MBZ: spin-orbit coupling opens band gaps [shaded green in (a)] that are absent in the Abelian model. (c) Inversion eigenvalues and the $\mathbb{Z}_2$ indices for all band gaps. (d), (e) Surface band structure cut along the (d) x and (e) z directions (with 20 magnetic unit cells) with remaining directions periodic. Surface states are highlighted in red.

therefore, the eigenspectrum of H doubles that of H_1. Regarding gapped phases, there are a total of four band gaps, half of which are chiral partners of the other half. As a result, we only need to examine the lowest two band gaps, whose strong and weak $\mathbb{Z}_2$ indices $(\nu_0; \nu_1, \nu_2, \nu_3)$ [35] (see Supplemental Material [31]) are shown in Table I, obtained via inversion

TABLE II. The strong and weak $\mathbb{Z}_2$ indices for $(\theta_x, \theta_y, \theta_z) = (2\pi/3, 2\pi/3, 0)$ for each gap are shown. Although this choice of gauge fields does not enable chiral symmetry in the system, the sublattice symmetry remains intact, which connects the topology of positive and negative band gaps [e.g., see inversion eigenvalues of gaps 3 and 6 in Fig. 3(c)].

Gap	Bands	ν_0	ν_1	ν_2	ν_3
1	6	1	1	1	1
2	12	1	1	1	1
3 (complete)	18	1	1	1	1
4	24	0	1	1	1
5	30	0	1	1	1
6 (complete)	36	1	0	0	0
7	42	1	0	0	0
8	48	1	0	0	0

eigenvalues at the eight time-reversal-invariant momenta [see Fig. 2(b)]. Because all its $\mathbb{Z}_2$ indices simultaneously vanish, the first gap around $E = -3$ is topologically trivial, as also supported by its trivial surface states in Fig. 2. On the other hand, the second gap, around $E = -1.5$, is a weak topological insulator (TI) (see Table I) with an odd index $\nu_2 = 1$. We confirm this weak-TI diagnosis with surface x-cut [Fig. 2(c)] and y-cut [Fig. 2(d)] calculations. The surface states of the second gap are nontrivial and trivial in the x-cut and y-cut systems, respectively. Meanwhile, the surface states of the first gap are trivial in both truncation directions. These surface states are consistent with the bulk diagnosis in Table I.

Next, we study $H_+(2\pi/3, 2\pi/3, 0)$. Evidently, this choice of hopping phases lies within the genuine non-Abelian regime. To highlight the associated consequence, we compare the bulk spectra of H_+ with that of the three-dimensional Abelian Hofstadter model $H_1(2\pi/3, 2\pi/3, 0)$ [Eq. (1)], as shown in Figs. 3(a) and 3(b), respectively, sampled along high-symmetry lines in the three-dimensional magnetic Brillouin zone. Compared to H_1 in Fig. 3(b), which is gapless, new band gaps (with complete band gaps shown in shaded blue) are opened in Fig. 3(a) due to the addition of spin-orbit coupling. A similar band-gap opening also appears for other choices of gauge fields (see Supplemental Material [31] Fig. S2). For $(\theta_x, \theta_y, \theta_z) = (2\pi/3, 2\pi/3, 0)$, the magnetic unit cell has dimensions $3 \times 3 \times 3$ with a total of 27 Kramers pairs. There are a total of eight band gaps with two complete ones (highlighted by green shadings in Fig. 3). The strong and weak $\mathbb{Z}_2$ indices $(\nu_0; \nu_1, \nu_2, \nu_3)$ are also evaluated for all band gaps using inversion eigenvalues [Fig. 3(c)] and shown in Table II. Evidently, the system is a strong 3D topological insulator at both the complete band gaps (namely, gaps 3 and 6). We also include the calculation of the Wannier spectrum with odd winding [36] (see Supplemental Material [31] Fig. S4), which affirms our results for $\mathbb{Z}_2$ invariants calculated using inversion eigenvalues. We verify such a bulk analysis by calculating the surface spectra with open boundary conditions in the x [Fig. 3(d)] and z [(Fig. 3(e)] directions. In contrast to those of the weak insulating phase shown in Fig. 2, the complete gaps of the strong insulating phase exhibit helical surface states under both types of truncation. Notably, with the x cut [Fig. 3(d)], the surface Dirac points appear at the T and Γ points for gaps 3 and 6, respectively, which is ensured by the sublattice symmetry of the Hamiltonian. A similar correspondence between the surface Dirac points appears also for the z-cut spectrum in Fig. 3(e).

V. CONCLUSION

In conclusion, we have introduced a three-dimensional non-Abelian generalization of the Hofstadter model with three spatially inhomogeneous and linearly varying gauge fields on a cubic lattice, proven the genuine non-Abelian condition of the model, analyzed its internal symmetries, and discussed the strong and weak $\mathbb{Z}_2$ insulating phases under different choices of gauge fields. Experimentally, it may be possible to realize the models on various platforms, including photonic coupled waveguide/resonator arrays and synthetic frequency combs, topological circuit systems, and spin-orbit-coupled atomic gases. Future directions also include analyzing the rich crystalline symmetries of the model and identifying the associated first-order and higher-order crystalline phases.

ACKNOWLEDGMENTS

We thank Liang Fu, Hoi Chun Po, and Ashvin Vishwanath for discussions. This material is based upon work supported in part by the Air Force Office of Scientific Research under Award No. FA9550-20-1-0115, as well as in part by the U.S. Office of Naval Research (ONR) Multidisciplinary University Research Initiative (MURI) Grant No. N00014-20-1-2325 on Robust Photonic Materials with High-Order Topological Protection. This material is also based upon work supported in part by the U. S. Army Research Office through the Institute for Soldier Nanotechnologies at MIT, under Collaborative Agreement No. W911NF-18-2-0048.

[1] D. R. Hofstadter, Phys. Rev. B **14**, 2239 (1976).
[2] C. R. Dean, L. Wang, P. Maher, C. Forsythe, F. Ghahari, Y. Gao, J. Katoch, M. Ishigami, P. Moon, M. Koshino *et al.*, Nature (London) **497**, 598 (2013).
[3] L. Ponomarenko, R. Gorbachev, G. Yu, D. Elias, R. Jalil, A. Patel, A. Mishchenko, A. Mayorov, C. Woods, J. Wallbank *et al.*, Nature (London) **497**, 594 (2013).
[4] B. Hunt, J. D. Sanchez-Yamagishi, A. F. Young, M. Yankowitz, B. J. LeRoy, K. Watanabe, T. Taniguchi, P. Moon, M. Koshino, P. Jarillo-Herrero *et al.*, Science **340**, 1427 (2013).
[5] M. Aidelsburger, S. Nascimbene, and N. Goldman, C. R. Phys. **19**, 394 (2018).
[6] U. Kuhl and H.-J. Stöckmann, Phys. Rev. Lett. **80**, 3232 (1998).
[7] M. Aidelsburger, M. Atala, M. Lohse, J. T. Barreiro, B. Paredes, and I. Bloch, Phys. Rev. Lett. **111**, 185301 (2013).
[8] H. Miyake, G. A. Siviloglou, C. J. Kennedy, W. C. Burton, and W. Ketterle, Phys. Rev. Lett. **111**, 185302 (2013).
[9] X. Ni, K. Chen, M. Weiner, D. J. Apigo, C. Prodan, A. Alù, E. Prodan, and A. B. Khanikaev, Commun. Phys. **2**, 55 (2019).

[10] M. Hafezi, S. Mittal, J. Fan, A. Migdall, and J. Taylor, Nat. Photonics **7**, 1001 (2013).
[11] P. Roushan, C. Neill, J. Tangpanitanon, V. Bastidas, A. Megrant, R. Barends, Y. Chen, Z. Chen, B. Chiaro, A. Dunsworth *et al.*, Science **358**, 1175 (2017).
[12] C. Owens, A. LaChapelle, B. Saxberg, B. M. Anderson, R. Ma, J. Simon, and D. I. Schuster, Phys. Rev. A **97**, 013818 (2018).
[13] K. Osterloh, M. Baig, L. Santos, P. Zoller, and M. Lewenstein, Phys. Rev. Lett. **95**, 010403 (2005).
[14] N. Goldman, A. Kubasiak, P. Gaspard, and M. Lewenstein, Phys. Rev. A **79**, 023624 (2009).
[15] M. Burrello and A. Trombettoni, Phys. Rev. Lett. **105**, 125304 (2010).
[16] A. Kosior and K. Sacha, Europhys. Lett. **107**, 26006 (2014).
[17] N. Goldman, I. Satija, P. Nikolic, A. Bermudez, M. A. Martin-Delgado, M. Lewenstein, and I. B. Spielman, Phys. Rev. Lett. **105**, 255302 (2010).
[18] Y. Yang, B. Zhen, J. D. Joannopoulos, and M. Soljačić, Light: Sci. Appl. **9**, 177 (2020).
[19] Y. Yang, C. Peng, D. Zhu, H. Buljan, J. D. Joannopoulos, B. Zhen, and M. Soljačić, Science **365**, 1021 (2019).
[20] T. T. Wu and C. N. Yang, Phys. Rev. D **12**, 3845 (1975).
[21] Y. Chen, R.-Y. Zhang, Z. Xiong, Z. H. Hang, J. Li, J. Q. Shen, and C. T. Chan, Nat. Commun. **10**, 3125 (2019).
[22] B. Zygelman, Phys. Rev. A **103**, 042212 (2021).
[23] T. Iadecola, T. Schuster, and C. Chamon, Phys. Rev. Lett. **117**, 073901 (2016).
[24] J. Noh, T. Schuster, T. Iadecola, S. Huang, M. Wang, K. P. Chen, C. Chamon, and M. C. Rechtsman, Nat. Phys. **16**, 989 (2020).
[25] Y. Hasegawa, J. Phys. Soc. Jpn. **59**, 4384 (1990).
[26] G. Montambaux and M. Kohmoto, Phys. Rev. B **41**, 11417 (1990).
[27] Z. Kunszt and A. Zee, Phys. Rev. B **44**, 6842 (1991).
[28] M. Kohmoto, B. I. Halperin, and Y.-S. Wu, Phys. Rev. B **45**, 13488 (1992).
[29] M. Koshino, H. Aoki, K. Kuroki, S. Kagoshima, and T. Osada, Phys. Rev. Lett. **86**, 1062 (2001).
[30] Y. Li, Phys. Rev. B **91**, 195133 (2015).
[31] See Supplemental Material at http://link.aps.org/supplemental/10.1103/PhysRevB.104.115127 for additional bulk spectra, chiral symmetry, and the calculations of topological indices and Wannier spectra.
[32] N. Goldman, A. Kubasiak, A. Bermudez, P. Gaspard, M. Lewenstein, and M. A. Martin-Delgado, Phys. Rev. Lett. **103**, 035301 (2009).
[33] N. Goldman, G. Juzeliūnas, P. Öhberg, and I. B. Spielman, Rep. Prog. Phys. **77**, 126401 (2014).
[34] X. Wen and A. Zee, Nucl. Phys. B **316**, 641 (1989).
[35] L. Fu and C. L. Kane, Phys. Rev. B **76**, 045302 (2007).
[36] A. A. Soluyanov and D. Vanderbilt, Phys. Rev. B **83**, 035108 (2011).